Published in final edited form as:
Appl Phys B. 2008 December 12; 94(4): 569–575. doi:10.1007/s00340-008-3342-6.

K_α x-ray emission characterization of 100 Hz, 15 mJ femtosecond laser system with high contrast ratio

S. Fourmaux,
INRS-EMT, Université du Québec, Varennes, J3X 1S2, Canada, fourmaux@emt.inrs.ca

C. Serbanescu,
INRS-EMT, Université du Québec, Varennes, J3X 1S2, Canada

R.E. Kincaid Jr.,
Syracuse University, Syracuse, NY, USA

A. Krol, and
SUNY Upstate Medical University, Syracuse, NY, USA

J.C. Kieffer
INRS-EMT, Université du Québec, Varennes, J3X 1S2, Canada

Abstract

We report K_α x-ray production with a high energy (110 mJ per pulse at 800 nm before compression/ 15 mJ at 400 nm after compression), high repetition rate (100 Hz), and high pulse contrast (better than 10^{-9} at 400 nm) laser system. To develop laser-based x-ray sources for biomedical imaging requires to use high-energy and high-power ultra-fast laser system where compression is achieved under vacuum. Using this type of laser system, we demonstrate long-term stability of the x-ray yield, conversion efficiency higher than 1.5×10^{-5} with a Mo target, and the x-ray spot size close to the optical focal spot. This high-repetition K_α x-ray source can be very useful for x-ray phase-contrast imaging.

1 Introduction

High-intensity and high-repetition ultrafast lasers allow producing high mean flux of quasi-monochromatic K_α x-ray radiation. When the laser pulse is focused on a solid target with intensity in the range of 10^{15}–10^{18} W/cm^2, plasma is produced where hot electrons are accelerated. They penetrate the cold target volume and generate K_α x-ray lines in addition to broad Bremsstrahlung spectra.

Ultrafast laser-based K_α x-ray sources are of high interest for biomedical imaging applications as their energy can be easily selected by changing the target material and the x-ray source size can be reduced below 10 μm thus allowing imaging with high spatial resolution. With such a small x-ray source size, phase contrast imaging can be achieved. One practical application of such a source is *in vivo* phase contrast micro Computed Tomography (micro-CT) of small animal soft tissue cancer models. Because the *in vivo* scan duration is limited (typically it should not exceed 60 minutes), it is critical to attain sufficiently high and stable average x-ray flux

Correspondence to: S. Fourmaux.

S. Fourmaux and C. Serbanescu contributed equally to this work.

PACS 52.38.Ph · 52.59Px · 52.50Jm

while keeping the x-ray source size small. One solution is to use high-contrast laser pulses and to increase the energy and the repetition rate of the laser system. In this context it has been proposed to build a laser for biomedical imaging with 100 TW of instantaneous power, 100 Hz repetition rate, and 400 W of average power (ASUR project) [1]. This is why after demonstrating the potential for phase contrast imaging with a 9 W (before compression), 10 Hz laser system [2], we decided to change to a 11 W, 100 Hz laser system to validate this approach and prove that constant x-ray yield could be achieved with such high thermal load on the optical components.

The first studies concerning laser-based K_α x-ray radiation sources have been performed with Nd:glass low-repetition-rate laser system exhibiting picosecond laser pulse duration [3], and the first sub-picosecond quantitative characterization of K_α x-ray emission has been realized by Rousse et al. with a 10 Hz dye laser system [4]. The optimum intensity has been shown to depend of the target material atomic number Z as follows: $I_{opt}(W/cm^2) = 7 \times 10^9 \cdot Z^{4.4}$, while the value of the maximum achievable conversion efficiency has been shown to decrease with the atomic number Z [5].

In recent years, K_α x-ray sources have been extensively studied with femtosecond laser systems operating from single-shot mode up to 5 kHz repetition rate. To our knowledge, no work has been reported on high conversion efficiency and high x-ray source brightness due to high repetition rate combined with a small x-ray source size (compared to the laser spot size) obtained for high-energy K_α x-ray radiation (e.g., using Ag or Mo as target materials) well suitable for biomedical x-ray imaging.

Several works have reported on the relationship between the laser pulse contrast ratio and the x-ray source size: it appears to be crucial to work with a high-contrast laser pulse ratio to keep the x-ray source size close to the laser focal spot size [4,6–9]. For instance, while high conversion efficiencies into K_α x-rays have been demonstrated using laser systems with low-contrast ratio [7,10–12], the sizes of these x-ray sources where from 4 to 8 times the laser focal spot size.

Higher-energy K_α x-ray photons from heavy metals such as Ag or Mo have been used in only a limited number of experimental works. Yu et al. produced K_α x-ray radiation with frequency doubled high-contrast laser using Ag target. The x-ray energy and the x-ray source size were of interest for biomedical imaging, but the repetition rate was too low for such applications [6]. High-energy 600 mJ and high-intensity 4×10^{18} W/cm^2 K_α x-ray radiation has been produced using Ag target resulting in 2×10^{-5} conversion efficiency, but the x-ray source size was 5 times larger, as compared to the 10 μm optical focal spot size [10]. This is again due to the large prepulse utilized in the experiments of 10^{-4} for picoseconds pedestal and 10^{-5} for nanosecond prepulses. Generation of K_α x-ray radiation using Mo targets has been reported with frequency-doubled high-energy (200 mJ) and high-intensity 10^{18} W/cm^2 range laser pulses. The x-ray source size measured was more than 3 times the optical focal spot size, and the repetition rate was only 10 Hz [2]. In this experiment, the effective source size was limited by the laser beam pointing stability and the precision of the target positioning system.

As mentioned before, an approach to achieve high x-ray brightness would be an increase in the repetition rate. Several researchers have used laser systems with high-repetition rates (ranging from 1 kHz up to 5 kHz) and with Cu or Ga targets. However, the relatively low energy of the K_α lines from these elements make these sources to be suited for x-ray diffraction measurements but not optimized for biomedical imaging [11,13–15].

Here, we report K_α x-ray production with a high-energy (110 mJ per pulse) and high-repetition rate (100 Hz) laser system to benchmark the path toward high-power ultrafast laser system where compression is achieved under vacuum. In this study we choose to frequency double

the laser pulse in order to enhance the laser pulse contrast ratio and to keep the x-ray source size close to the laser spot size. We demonstrate long-term stability of the x-ray yield (hence the longterm stability of the x-ray flux), conversion efficiency higher than 1.5×10^{-5} with a high *Z* Mo target, and the x-ray spot size close to the optical focal spot.

2 Experimental set-up

This experimental study took place at the Advanced Laser Light Source (ALLS) Canadian facility [16]. Description of the ALLS 100 Hz laser system can be found elsewhere [17]. The laser is a commercial prototype built by Thalès Laser. It is based on Ti:Sapphire amplification crystals and the chirp pulse amplification (CPA) technique. This system produces laser pulses at 800 nm fundamental frequency with 100 Hz repetition rate, 35 fs pulse duration, and a maximum 70 mJ energy after compression. The incident average power on the compressor grating is 11 W.

The laser pulse contrast ratio at the fundamental frequency is measured to be better than 10^{-5} both in the nanosecond time range and in the picosecond time range for a delay higher than 5 ps before the main pulse. These data are respectively obtained using a fast photodiode using calibrated neutral density filters and a third-order autocorrelator. At 1 ps delay before the main pulse, the laser pulse contrast ratio is 4×10^{-5}. To improve the laser pulse contrast ratio we chose, after compression, to frequency double the laser pulse with a Type I, 1-mm-thick KDP crystal. The measured conversion efficiency was 20% that reduced the average laser power down to 1.5 W on the target. The frequency-doubled laser pulse contrast ratio is not measured but deduced from the laser pulse contrast ratio at 800 nm. Based on previous studies, we estimated it to be better than 10^{-9} at 400 nm [6,18–20].

The 400 nm beam is focused on a molybdenum solid target into a 7.5 μm diameter FWHM focal spot, by the use of an *f*/3 off-axis parabola, resulting in a peak intensity of 8×10^{17} W/cm^2 on the target. Thus, for the same focusing conditions, the prepulses are focused to intensities lower than 10^9 W/cm^2, which is below the ablation threshold for metals. A permanent imaging system consisting of a lens $f = 10$ cm and a CCD camera 2.5 m away with a 10× microscope objective allowed us to monitor the beam focal spot on the target location with a 45× magnification. The target was moved continuously in order to get the beam interacting with clean surface at each laser shot. The target holder allowed us to insure that at each laser shot the target position was within 10 μm precision from the focal spot along the laser axis. The target holder could be translated under vacuum to allow the beam to propagate at maximum energy into the imaging system or to set the target in position for laser plasma interaction. A protective fused silica thin plate was used in front of the off-axis parabola focusing optics to avoid any coating that may result in the degradation of the parabola and in the decrease of the x-ray yield.

Figure 1 shows the experimental configuration in the target vacuum chamber. The laser is not fully *P* -polarized due to geometric constraints, i.e., this interaction chamber was not originally dedicated to K_α x-ray production [17].

X-rays produced by the targets were monitored with two identical PMT filtered by a beryllium (Be) window and symmetrically (at a half angle of 4° around the equatorial plane) positioned outside of the vacuum chamber at a distance of 62 cm. The x-ray spectra were measured with a CdZnTe detector (Amptek) positioned at 60 cm distance from the target (35 cm in air) and 8° in relation to the imaging axis (*Z*-axis on Fig. 1). This detector had a light-tight vacuum Be window with 10 mil thickness. The signal from the CdZnTe detector was amplified in a preamplifier (Amptek) and finally fed into a multi-channel analyser MCA (micro-ACE, Ortec). The whole detection system was calibrated with Am-241 radiation source at 13.95 keV and 59.54 keV. X-ray source size was measured using the cooled PI-SCX4300 (Roper Scientific)

Charge-Coupled Device (CCD) camera. This CCD has a 50 × 50 mm field-of-view and 2084 × 2084 pixel CCD chip. The pixel size is 24 μm. The camera offers 16 bits of digitization. For convenient coupling of scintillator screens to the CCD, a 1 : 1 fiber-optic faceplate is permanently bonded to the chip. This faceplate isolates the CD, which is placed under vacuum. For x-ray imaging, the camera was coupled to a Gd_2SO_2 scin-tillator.

3 Results and discussion

The laser focal spot observed with the imaging system is shown in Fig. 2. In the air and at low energy the spot size dimensions were 7.2±0.3 × 7.1±0.3 μm FWHM (Fig. 2a). Under vacuum and for 10% energy, the spot size dimension was similar: 7.5 × 7.4 μm FWHM (Fig. 2b). When the laser pulse energy was increased up to its maximum value, we observed a laser beam distortion due to 11W thermal loading of the compressor grating under vacuum (Fig. 2c) [21]. This distortion was mainly defocussing and resulted in a 500 μm displacement of the focal spot position opposite to the direction of the laser propagation vector. The 3-axis off-axis parabola holder was motorized to allow correction of this defocussing, and the resulting corrected spot size was 6.9×7.4 μm FWHM (Fig. 2d).

The CdZnTe detector was operated for 300 s to acquire the x-ray source spectrum displayed in Fig. 3. Due to some beamtime sharing constraints at ALLS facility, the laser was operated in two modes: (a) using 110 mJ maximal energy before compression, resulting in 15 mJ at 400 nm incident on target; (b) using 90 mJ maximal energy before compression, resulting in 9 mJ at 400 nm incident on target. Figure 3 shows the resulting spectra depending of the laser beam energy and the operation mode of the laser (with and without correction of the heat induced distortion).

The laser beam was inserted into the experimental system by means of a mechanical shutter located at the entrance of the compressor vacuum chamber. When the alignment was achieved at low energy and we let the beam propagate for 300 s onto the target, we obtained 1.5×10^{-5} conversion efficiency into K_α x-rays (using 110 mJ energy before compression) with 27.9% of the detected photons in the K_α lines. Using 90 mJ energy before compression, we measured 5×10^{-6} conversion efficiency into K_α x-rays. The laser peak intensities were 8×10^{17} W/cm^2 and 5×10^{17} W/cm^2, respectively. During 300 s accumulation time, we observed an increase of the soft x-rays counts, as compared to the hard x-rays counts after 90 s of acquisition. This was consistent with the decrease in the laser intensity due to laser focal spot distortion. After 30 s of operation, we also observed a signal decrease of the two PMT detectors, and after 90 s, their values became 25% of their initial values. As deduced from the x-ray spectra, the K_α x-ray source brightness was 1.2×10^9 ph/(sr s) and 2.8×10^8 ph/(sr s) for 110 and 90 mJ energy, respectively, at the compressor entrance.

When the alignment was achieved at high energy and the laser beam focal spot was compensated for thermal effects, we achieved 1.5×10^{-5} conversion efficiency (at 90 mJ energy) with 31.4% of the photons in the K_α lines. The source brightness was 8.3e8 ph/(sr s). By using such a procedure, the PMT value remained constant during the entire measurement. As the conversion efficiency ratio between 110 and 90 mJ input energies is a factor of three when the distortion of the laser beam due to thermal effect is not corrected, we may expect a similar increase between the two cases where correction is applied resulting in a source brightness of 4.2×10^9 ph/(sr s). A summary of the measured conversion efficiency for the cases presented up to now is displayed in Fig. 4. All results are reported in terms of energy conversion efficiency into 2π sr assuming isotropic emission. The solid diamond points correspond to the case where the laser beam focal spot was not compensated for thermal effects. The solid square point is the result obtained when the thermal induced distortion was corrected, and an increase in the conversion efficiency was observed for the same laser energy incident

on the target. The figure includes also a collection of the K_α x-ray measurements made with high-contrast femtosecond laser pulses using other laser systems. These measurements are represented by open squares. Each number inside the square denotes the reference number.

Figure 5 displays the image of a tungsten edge obtained after 5 minute accumulation time. From the edge profile we deduced that the x-ray source size was 8.5 × 16 μm FWHM. Due to the experimental geometry, the laser focal spot was projected onto the target resulting in 6.9 × 8.8 μm FWHM dimensions. Thus, the x-ray source size was only 1.2×1.8 times greater than the laser focal spot size. Such an x-ray source size confirms the high applicability for phase-contrast x-ray imaging applications.

Several studies already mentioned the crucial role of the laser pulse contrast to obtain small x-ray source size. If the prepulse intensity is above the target ablation threshold, then the main laser pulse will interact with the preformed plasma formed by the prepulse instead of the fresh target surface. Because the laser plasma interaction is very sensitive to the plasma density profile, the prepulse can influence significantly the outcome of the interaction. This is because a large prepulse will produce a long preplasma, where very energetic hot electrons can be generated, which are not desirable because they undergo larger trajectories away from the initial focal spot, resulting in an elongated x-ray pulse duration and spatial size. In our intensity regime the pulse contrast is high enough to prevent any pre-plasma production before the arrival of the main pulse. It leads us to estimate that the plasma density gradient L/λ is very steep and less than 0.2 [22]. Eder et al. [7] show that with respectively $L/\lambda = 0.4$ at 800 nm the x-ray spot size is found to be 9 times larger than the laser focal spot, while with $L/\lambda = 0.2$ at 400 nm the x-ray spot is found to be 4 times larger than the laser focal spot. In our experiment L/λ is less than 0.2, and an x-ray spot size less than 2 times larger than the laser focal spot is in a good agreement.

To explain the role of the laser pulse contrast to maintain the x-ray source size close to the focal spot size, several mechanisms have been invoked. Increase of the x-ray source size have been explained by Reich et al. by the presence of a magnetic field generated by pre-pulses which reflects a large portion of the hot electrons. The ponderomotive force can then spread the reflected hot electrons over a wider area of the target surface [23]. Another possible explanation for the large x-ray spot size observed in previous work has been associated with the low-intensity wings of the incident laser with an expected scaling of the hot-electron temperature from the pulse maximum to its edge, but in our experimental condition we estimate the hot-electron temperature to be 13 keV, which reduces the scattering electron length and such effect [7]. More studies would be necessary to fully understand the hot-electron transport through the target and its influence on the x-ray source size, but this is beyond the scope of this article.

This work sets a benchmark for the future high-energy high-power femtosecond laser-based x-ray imaging applications. Today two techniques are available to enhance the laser pulse contrast ratio at the fundamental frequency up to a level similar to the one we obtained by frequency doubling: cross-polarized wave (XPW) generation [24] and booster amplifier [25]. This would allow using 70 mJ laser pulses on target instead of only 15 mJ. The use of laser pulses with energies of 70 mJ would result in an increase of laser intensity by a factor of almost 5 times for the same focusing conditions. For application purposes, it is useful to know how many K_α x-ray photons can be obtained under given working conditions. Reich et al. [5] theoretically determined that there is an optimum laser intensity range for a given material to obtain maximum conversion efficiency into K_α x-rays. For high Z target materials, this optimum laser intensity was found to be in the 5×10^{17}–10^{19} W/cm^2 intensity range. Based on these predictions, we conservatively assume that the K_α x-ray conversion efficiency obtained from 70 mJ laser pulses to be similar to the one we have measured in of 1.5×10^{-5}. In this

case, an image with 10% photon noise per pixel with the detector located at 1 m distance would take 27 s instead of 3.5 minutes in the current measured conditions (thermal-induced distortion corrected and 9 mJ incident on target). A complete tomographic scan consisting of 360 images would take 2.7 h instead of 21 h. It should also be noted that the laser polarization could be improved to further increase of the x-ray flux. It could be accomplished by optimization of the experimental set up.

4 Conclusion

We reported the first demonstration of long-term stability of the x-ray yield of K_α x-ray production with a high-energy and high-repetition rate laser system. This confirms the great potential of laser-based x-ray source for biomedical imaging that will require high-energy and high-power ultrafast laser system where compression is achieved under vacuum. We demonstrated conversion efficiency higher than 1.5×10^{-5} with a high Z Mo target, and the x-ray spot size close to the optical focal spot.

Acknowledgments

The authors would like to thank Marina Servol and Rémy Toth for helpful discussion. The authors gratefully acknowledge INRS-EMT and ALLS technical team for their supports during the experiments: Lukasz Andrzejewski, Antoine Laramée, Guy Lebrun, Carol Morisette, Léonard Pelletier, Claude Sirois, and François Poitras. The ALLS facility has been founded by the Canadian Foundation for Innovation (CFI). This research has been supported in part by grant EB005055-01A1 from the National Institute of Biomedical Imaging and Bioengineering, NIH. This work is founded by NSERC, the Canada Research Chair Program and by Ministère de l'Éducation du Québec.

References

1. Kieffer, JC. CAP Congress. Université Laval; 2008.
2. Toth R, Kieffer JC, Fourmaux S, et al. Rev. Sci. Instrum 2005;76:083701.
3. Chen H, Soom B, Yaakobi B, et al. Phys. Rev. Lett 1993;70:3431. [PubMed: 10053867]
4. Rousse A, Audebert P, Geindre JP, et al. Phys. Rev. E 1994;50:2200.
5. Reich, Ch; Gibbon, P.; Uschmann, I.; Foster, E. Phys. Rev. Lett 2000;84:4846. [PubMed: 10990813]
6. Yu J, Jiang Z, Kieffer JC, Krol A. Phys. Plasmas 1999;6:1318.
7. Eder DC, Pretzler G, Fill E, et al. Appl. Phys. B 2000;70:211.
8. Zhavoronkov N, Gritsai Y, Korn G, Elsaesser T. Appl. Phys. B 2004;79:663.
9. Toth R, Fourmaux S, Ozaki T, et al. Phys. Plasmas 2007;14:053506.
10. Chen LM, Forget P, Fourmaux S, et al. Phys. Plasmas 2004;11:4439.
11. Serbanescu CG, Chakera JA, Fedosejevs R. Rev. Sci. Instrum 2007;78:103502. [PubMed: 17979414]
12. Boschetto D, Mourou G, Rousse A, et al. Appl. Phys. Lett 2007;90:011106.
13. Korn G, Thoss A, Stiel H, et al. Opt. Lett 2002;27:866. [PubMed: 18007954]
14. Jiang Y, Lee T, Li W, et al. Opt. Lett 2002;27:963. [PubMed: 18026338]
15. Bonvalet A, Darmon A, Lambry JC, et al. Opt. Lett 2006;31:2753. [PubMed: 16936881]
16. ALLS. Annual Report 2005–2006. 2006.
17. Fourmaux S, Lecherbourg L, Harmand M, et al. Rev. Sci. Instrum 2007;78:113104. [PubMed: 18052462]
18. Anderson E, Holzer G, Foster E, et al. J. Appl. Phys 2001;90:3048.
19. Yasuike K, Key M, Hatchett SP, et al. Rev. Sci. Instrum 2001;72:1236.
20. Price DF, More RM, Walling RS, Guethlein G, Shepherd RL, Stewart RE, White WE. Phys. Rev. Letters 1995;75:252.
21. Fourmaux S, Serbanescu C, Lecherbourg L, et al. Opt. Express. (accepted).
22. Zepf M, Tsakiris GD, Pretzler G, et al. Phys. Rev. E 1998;58:R5253.
23. Reich, Ch; Uschmann, I.; Ewald, F., et al. Phys. Rev. E 2003;68:056408.

24. Jullien A, Albert O, Burgy F, et al. Opt. Lett 2005;30:920. [PubMed: 15865399]
25. Fourmaux S, Payeur S, Alexandrov A, et al. Opt. Express 2008;16:11987. [PubMed: 18679471]

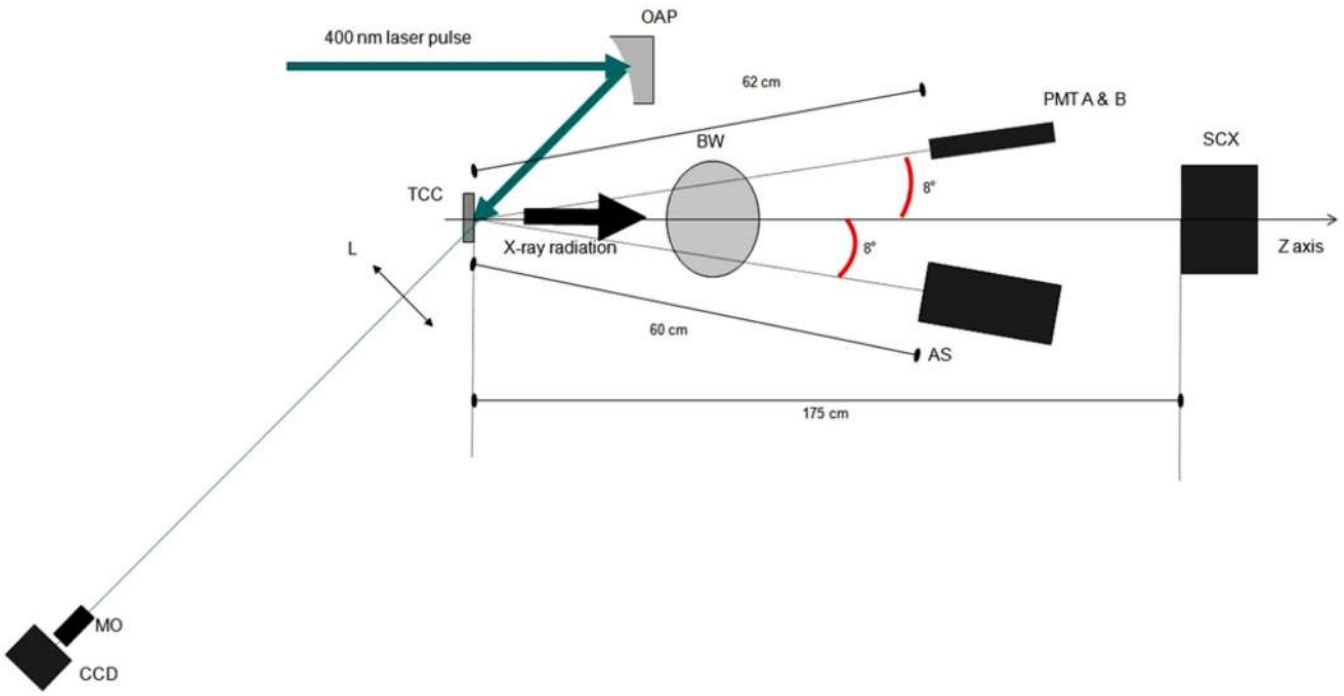

Fig. 1.

Schematic experimental setup. The 400 nm laser beam is represented by the turquoise lines. OAP, off-axis parabola; TCC, target chamber center. The x-ray diagnostics disposed outside the target chamber and filtered by a Be window (BW) are shown: the two symmetrically disposed PMT detectors (PMT A and PMT B); AS, CdZnTe detector for spectrum measurement; SCX, imaging x-ray CCD camera for source size measurement. The *Z*-axis shows the imaging direction of this camera. We also show the configuration of the imaging system (not at real scale) with: *L*, $f = +10$ cm lens; MO, ×10 microscope objective; CCD, far-field monitor CCD

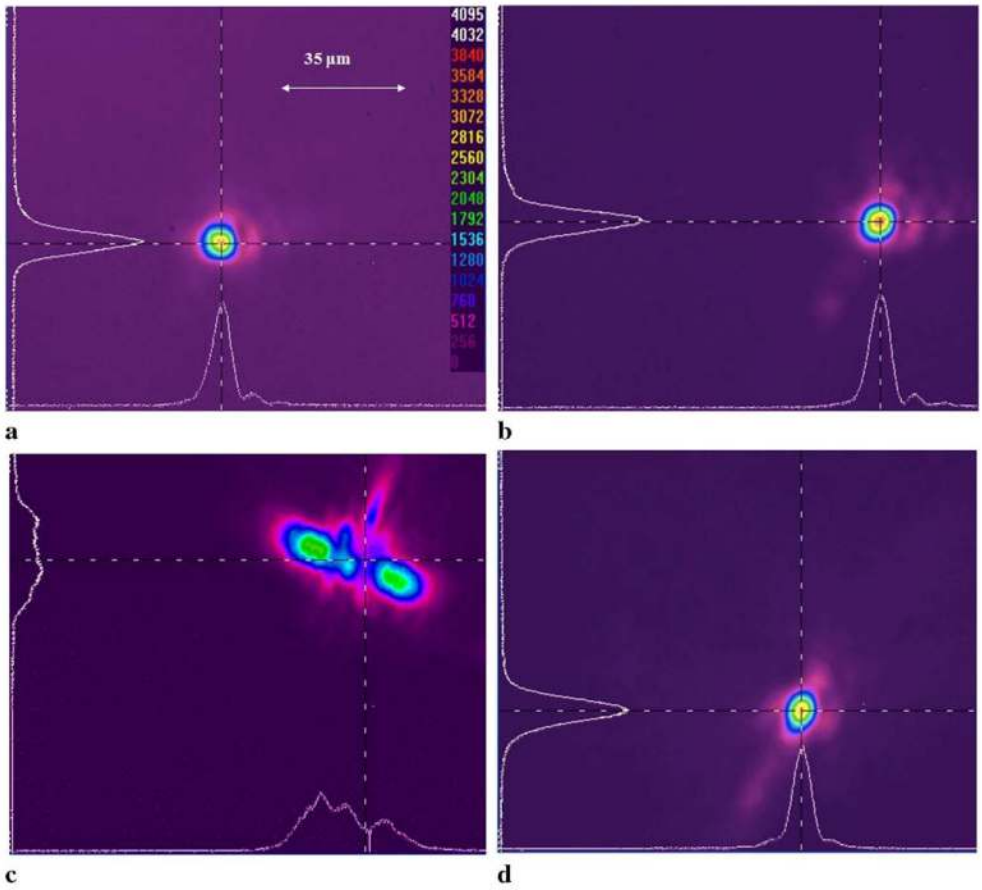

Fig. 2.

Measurement of the beam shape with the imaging system. The lens image the plane corresponding to the target chamber center (TCC). **a** Focal spot after alignment at air and low energy. **b** Focal spot under vacuum and 10% energy. **c** Beam shape evolution after 100 s at 100% energy. **d** Focal spot obtained after moving the off axis parabola along the laser axis to compensate for the thermal-induced distortion

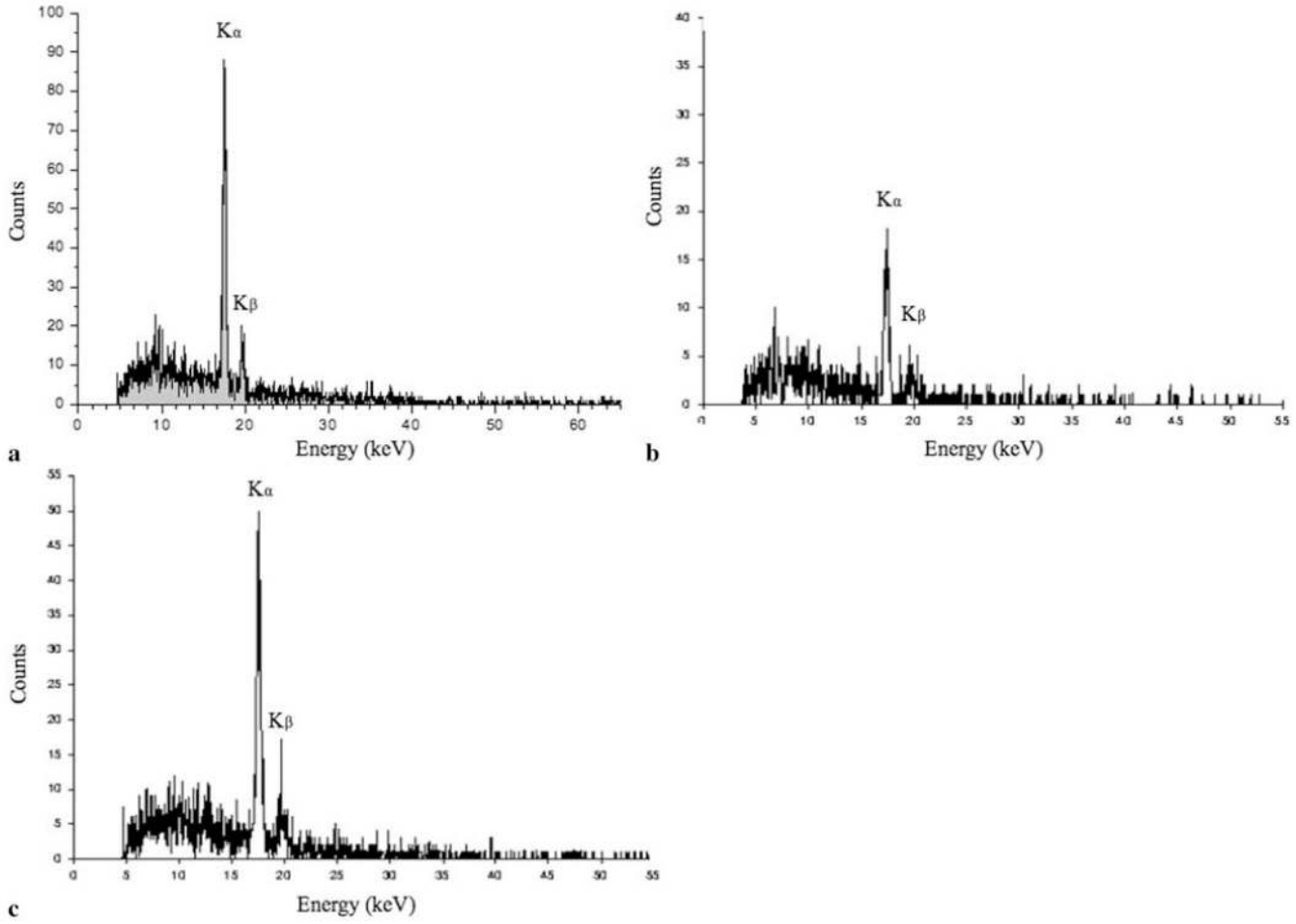

Fig. 3.

CdZnTe detector spectra. **a** Obtained with 110 mJ before compression and no correction for the thermally induced effects (laser beam focal spot is align at air and low energy). **b** Obtained with 90 mJ before compression and no correction for the thermally induced effect. **c** Obtained with 90 mJ before compression and with compensation for the thermally induced effect (beam is propagated through the experimental system until a steady state for the thermal loading is reached, then the focal spot is corrected by moving the off axis parabola)

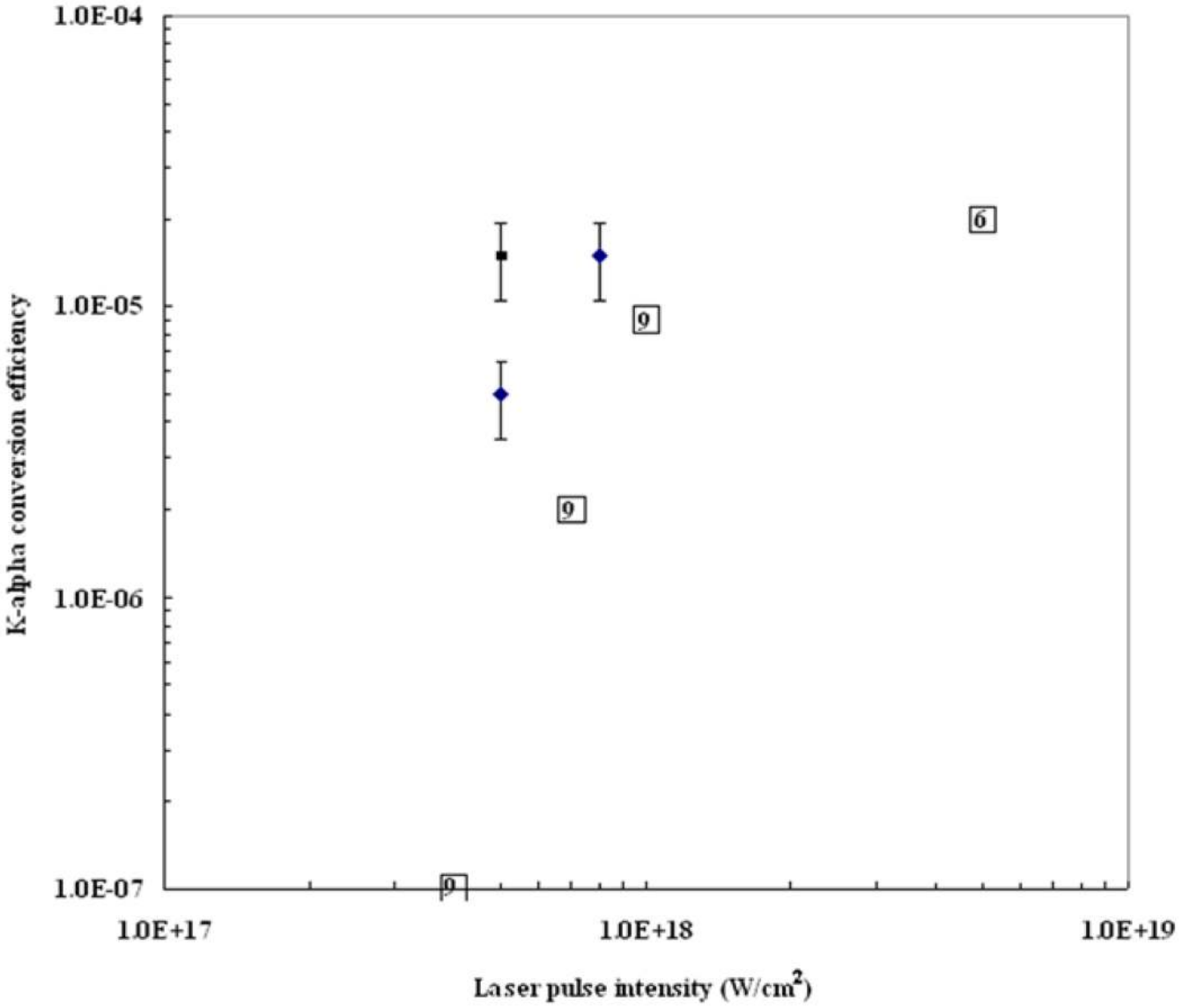

Fig. 4.

Summary of the current x-ray experimental results (*solid points*). The *solid diamond points* represent the results obtained with laser pulses with no corrections applied to compensate the laser beam distortion due to thermal effects. The *solid square point* is the result obtained when the laser focal spot was compensated for thermal effects. The *open squares* represent other measurements obtained with high-contrast femtosecond laser pulses. Each *number inside the square* denotes the reference number

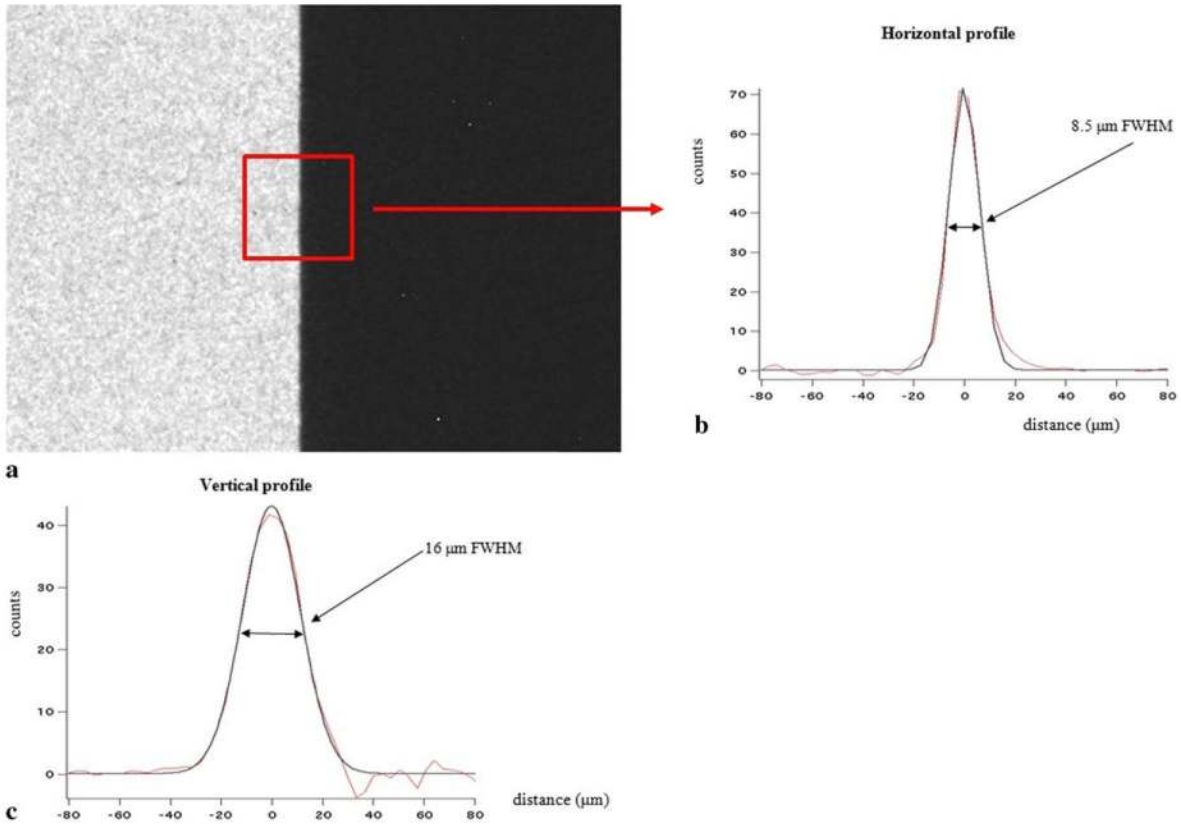

Fig. 5.

X-ray imaging of a Tungsten edge. The edge is positioned at 25 cm from the x-ray source. The SCX CCD is positioned 175 cm from the x-ray source. **a** Picture showing the lateral edge. **b** Differentiation of the lateral edge profile and Gaussian fit. **c** Differentiation of the vertical edge profile and Gaussian fit